Strong coupling with light enhances the photoisomerization quantum yield of azobenzene

J. Fregoni,[1,2] G. Granucci,[3*] M. Persico,[3] S. Corni[2,4*]

[1] Dipartimento di Scienze Fisiche, Informatiche e Matematiche, Università of Modena and Reggio Emilia, I-41125 Modena, Italy

[2] Istituto Nanoscienze, Consiglio Nazionale delle Ricerche CNR-NANO, I-41125 Modena, Italy

[3] Dipartimento di Chimica e Chimica Industriale, Università di Pisa, I-56124 Pisa, Italy

[4] Dipartimento di Scienze Chimiche, Università di Padova, I-35131 Padova, Italy

[*] E-mail: stefano.corni@unipd.it, giovanni.granucci@unipi.it

The strong coupling between molecules and photons in resonant cavities offers a new toolbox to manipulate photochemical reactions. While the quenching of photochemical reactions in the strong coupling regime has been demonstrated before, their enhancement has proven to be more elusive. By means of a state-of-the-art approach, here we show how the *trans*→*cis* photoisomerization quantum yield of azobenzene embedded in a realistic environment can be higher in polaritonic conditions than in the cavity-free case. We characterize the mechanism leading to such enhancement and discuss the conditions to push the photostationary state towards the unfavoured reaction product. Our results provide a signature that the control of photochemical reactions through

strong coupling can be extended from selective quenching to improvement of the quantum yields.

Introduction

The interaction between light and matter at the nanoscale is at the basis of a manifold of experimental applications in plasmonics[1, 2, 3, 4], single-molecule spectroscopies[5, 6], nanoprinting[7] and nanocavity optics[8, 9, 10]. When light is sufficiently confined in micro/nanometric systems in presence of one or more quantum emitters, its exchange of energy with the emitters becomes coherent and the system enters the strong coupling regime[11, 12]. Accordingly, the degrees of freedom of light and matter mix and the states of the system are described as hybrids between the two: the polaritons[13, 14]. The first experimental realizations to pioneer the idea of controlling the chemical reactions through strong coupling of molecules with light made use of metallic cavities.[15, 16]. Later on, the achievement of strong coupling with plasmonic nanocavities at the single-molecule level at room temperature has been obtained with a Nanoparticle on a Mirror (NPoM) setup[17, 18]. Such setup has been recently improved with DNA origami for higher reproducibility [19, 20]. The manifold of possibilities opened up by such experiments drove efforts to explore microcavities-based setups at low temperature, achieving longer lifetimes for the whole system[21]. Theoretical modeling followed immediately to survey the plethora of new possibilities offered by strong light-molecule coupling[22, 23]. The high flexibility of the polaritonic properties has been assessed for both realized[24, 25, 20] and potential applications[13, 26] giving birth to a class of new branch of chemistry[27]: the so-called polaritonic chemistry.[28]

When a resonant mode is coupled to electronic transitions, the molecules exhibit enhanced spontaneous emission at both the collective and single molecule level[29, 30, 31, 32]. The

enhanced emission is experimentally exploited in confined systems to allow coherent energy exchange between light and photoactive molecules, potentially translating into modified photochemical properties[15]. The modifications to the potential energy surfaces (PESs through all the current work) driving different photophysical and photochemical behaviours are described by a basis of direct products of electronic and photonic states. Under this assumption, the states of the system are best described as hybrids between electronic and photonic.[12, 14, 33].

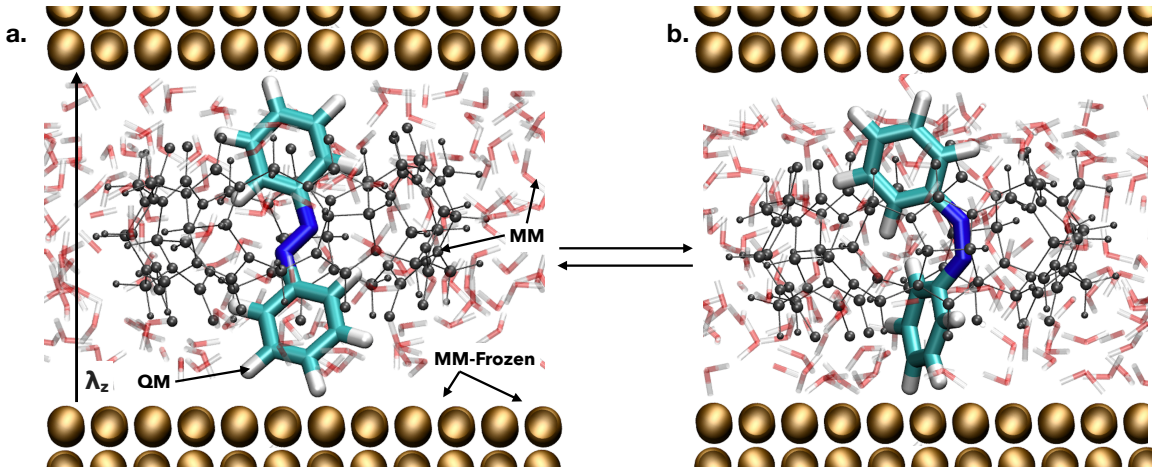

Figure 1: **Simulated system** Snapshots of the simulated system mimicking a plasmonic nanocavity as the one reported by Baumberg and coworkers[17]. The molecule, here azobenzene in *trans* (panel **a**) or *cis* (panel **b**) configurations, is computed at QM level (see text and Methods) and interacts with the MM environment by electrostatic embedding plus Lennard-Jones potentials. The environment is composed by cucurbit-7-uril (grey organic molecule cage) and gold layers (four layers on each side, frozen MM degrees of freedom), including also explicit water molecules. The cavity mode is polarized along $\boldsymbol{\lambda}_z$ and the sampling is run at room temperature[34].

The possibility to shape the electronic states with quantum light inspired various groups to explore the role of strong light-molecule coupling in controlling photochemical processes. For collective effects, the focus has been on polariton formation in full quantum diatomic molecules[35] and on several model dye molecules in a realistic environment[36]. At the single molecule level, the non-adiabatic dynamics schemes developed allowed to predict fea-

tures arising on the PESs like the creation of avoided crossings and light-induced conical intersections[13, 37, 38]. Such features modify the shape of PESs, translating into a potentially different photochemical reactivity[27, 39, 40]. The possibility to enhance the yield of photochemical processes has been recently proven for energy transfer[41], singlet fission[40] and catalysed reactions through vibrational strong coupling, obtained by exploiting remote catalysts[42]. For strong coupling with resonant optical frequencies, enhancement has only been suggested based on calculation on model PESs[28, 43] and neglecting the cavity losses and realistic non-radiative events.

As such events play a central role in the yields of photochemical reactions, the question remains if strong coupling can lead to a real enhancement of photochemical quantum yields in real molecules. Even more practically, the interest resides in the photostationary regime and in determining whether the related concentrations of products is enriched with respect to the standard reaction conditions. Here, by means of the state-of the art approach we devised[44], we show that it is possible to identify conditions that lead to improved quantum yields and product-enriched photostationary states. By investigating azobenzene *trans*→*cis* photoisomerization in strong coupling, we compare to the zero coupling case and highlight the differences between the two processes. Such comparison allows us to propose an interpretation of the mechanism leading to the increased quantum yield for the *trans*→*cis* $\pi - \pi^*$ photoisomerization.

The model system we simulate is depicted in Figure 1 and mimics the experimental setup used by Baumberg and coworkers[17] for achieving strong coupling with a single methylene blue chromophore. The azobenzene molecules are hosted in a one-to-one arrangement by cucurbit-7-uril ring molecules, which are in turn adsorbed on a planar gold surface. In this arrangement, the azobenzene long axis is approximately perpendicular to the surface. This is

relevant because the field polarization, the transition dipoles for the S_0-S_1 transition and the transition dipole for the S_0-S_2 transition are all aligned in the same direction[45]. The cavity is completed by gold nanoparticles sitting on top of the cucurbituril ring and much larger than the latter, so we simulate them as a second planar surface. Explicit water molecules fill the space between the gold layers (see Supplementary Note 1).

Results

Polaritons in azobenzene

Before investigating the photochemical properties of molecules under strong coupling, we show how the coupling conditions affect the energy landscape in the case of multiple electronic states. In this section, we aim only to provide an interpretative framework for the results of next section, hence the results presented in this section are computed without environment.

In Figure 2 we present two relevant cuts of the polaritonic PESs for the isolated azobenzene molecule, one along the CNNC dihedral and the other along the symmetric NNC bending (symNNC). In the former, all other degrees of freedom and also symNNC were optimized for the ground state. In the latter, the analogous constrained optimization was done for each symNNC value, except that CNNC was fixed at 165°. We shall exploit the PESs presented in this section to act as a qualitative and conceptual aid. By doing so, we introduce the framework to discuss the mechanism leading to the enhanced yield of the photoisomerization reaction.

Even in absence of environment, when a single molecule is strongly coupled with a cavity, polaritons drastically affect its PESs[12, 13, 44]. The photochemical properties are, in turn, deeply affected by the shape of the polaritonic PESs. Aiming to thoroughly describe the molecule in the strong coupling regime, we build the polaritonic Hamiltonian in the framework

of a semiempirical wavefunction method[46]:

$$\hat{H}_{tot} = \hat{H}_{mol} + \hat{H}_{cav} + \hat{H}^{sc}_{int}. \tag{1}$$

Here $\hat{H}_{mol}$ is the semiempirical electronic Hamiltonian, $\hat{H}_{cav}$ is the quantized electromagnetic field Hamiltonian for an effective resonant mode set at optical frequencies and $\hat{H}^{sc}_{int}$ is the quantum interaction between light and molecule in a dipolar fashion:

$$\hat{H}^{sc}_{int} = E_{1ph} \sum_{n \neq n'} |n\rangle \boldsymbol{\lambda} \cdot \boldsymbol{\mu}(\boldsymbol{R})_{n,n'} \langle n'| \left(\hat{b}^{\dagger} + \hat{b}\right). \tag{2}$$

E_{1ph} represents the magnitude of the single-photon electric field of the confined light mode, $\boldsymbol{\mu}_{\mathrm{n,n'}}$ is the transition dipole moment between the electronic states, $\boldsymbol{\lambda}$ is the field polarization unit vector, $\hat{b}^{\dagger}$ and $\hat{b}$ are the bosonic creation and annihilation operators. The nuclear motion is treated classically, using the surface-hopping approach[44] (see Methods). By relying on a semiempirical wavefunction method, we provide a detailed description of the electronic structure at low computational cost. Such electronic structure method exploits a solid parameterization [47] of the semiempirical electronic Hamiltonian and has been previously validated against experimental data in a number of applications[48, 49, 50, 51].

To gain more insight on the polaritonic PESs features, we refer to the basis of uncoupled products of light and matter wavefunctions, given by the diagonalization of $\hat{H}_{mol} + \hat{H}_{cav}$, labeled as $|n, p\rangle$. Here, n (*e.g.* S_0, S_1) is the electronic state index and p is the photon occupation number, either 0 or 1 in the present work. We consider a cavity photon of frequency 2.8 eV. Therefore, states with $p \geq 2$ lay at least 5.6 eV higher in energy than the ground state, *i.e.* more than 1 eV above our excitation window, which reaches up to 4.5 eV. Due to such high energy difference, they cannot be populated during the dynamics and therefore they are disregarded

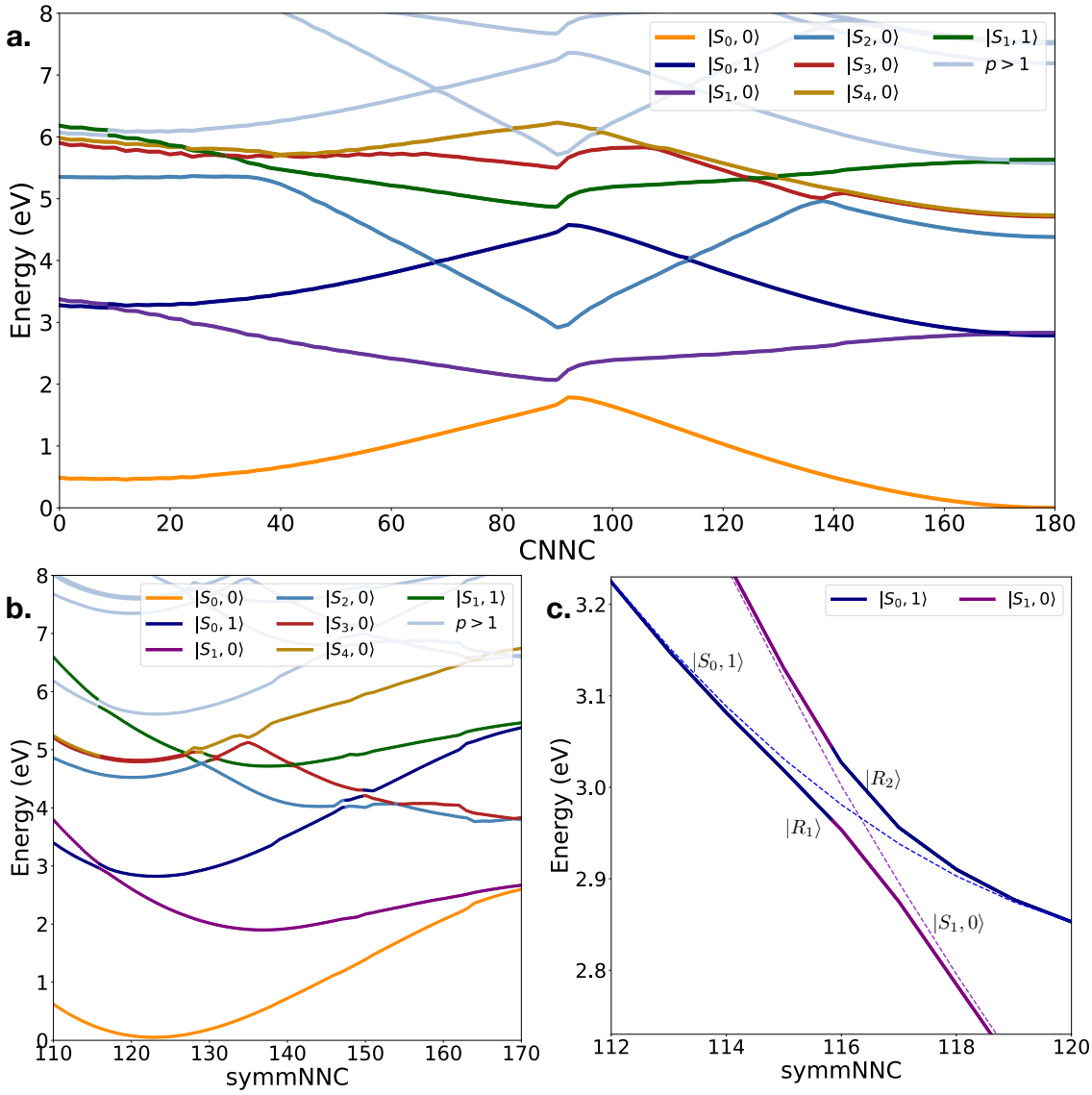

Figure 2: **Polaritonic potential energy curves of azobenzene with photon of 2.8 eV and single-photon electric field strength E_{1ph} of 0.002 a.u.** The polaritonic PESs are computed at the **a)** CNNC coordinate computed relaxing all the other degrees of freedom for the ground state and **b)** symNNC coordinate at CNNC 165° and constrained optimization as before. Each polaritonic branch is colored depending on the uncoupled state that majorly composes the polariton at each geometry. **c)** Detail of the strong coupling avoided crossing along the symNNC coordinate, with highlight of the $|S_0,1\rangle$ and $|S_1,0\rangle$ states which drive a different mechanism for the photoisomerization.

in our simulations (see Supplementary Note 2). To clearly distinguish the uncoupled states in strong coupling and the electronic states in the zero coupling frameworks, we refer to the set of uncoupled states $\{|n,p\rangle\}$ with the ket notation, *e.g.* $|S_0,1\rangle$ or $|S_1,0\rangle$, whereas the zero coupling electronic states $\{n\}$ are named by the state label only, *e.g.* S_0, S_1. The polaritonic eigenstates of $\hat{H}_{tot}$, labelled as $|R_k\rangle$, are expressed in the $|n,p\rangle$ basis:

$$|R_k\rangle = \sum_{n,p} D^k_{n,p}|n,p\rangle. \tag{3}$$

The coefficients $D^k_{n,p}$ of the uncoupled states in the wavefunction provide a simple interpretation for the system under strong coupling. The states with $p = 0$ represent all the cavity photon absorbed by the molecule, the states with $p = 1$ represent one free photon in the cavity and so on. In turn, the time-dependent polaritonic wavefunction can be expressed in either the polaritonic or the uncoupled basis set:

$$|\Psi(t)\rangle = \sum_k C_k(t)|R_k\rangle = \sum_k C_k(t)\sum_{n,p} D^k_{n,p}|n,p\rangle. \tag{4}$$

By the inclusion of the light-molecule interaction, a polaritonic avoided crossing or conical intersection is originated where the uncoupled states would cross. In Figure 2, we show such crossing along the two reactive coordinates: the torsion of the CNNC dihedral and the symNNC respectively. Here, the states labeled as $p > 1$ are included in the PESs calculations, yet they are not included in the dynamics presented in the next section.

The Rabi splitting between the polaritonic states is proportional to the transition dipole moment between the electronic states at the correspondent crossing geometry for the uncoupled states through eq. 2. The magnitude of such splitting represents the coherent energy exchange rate between light and molecule in a confined system. In Figure 2c we focus on the polaritonic

avoided crossing laying in the trans region (CNNC 165°). We anticipate that such crossing deeply impacts the photoisomerization mechanism of azobenzene, leading to enhanced trans-cis photoisomerization quantum yield.

Photochemistry on polaritonic states: tuning the photostationary equilibrium

In photoreversible processes, the ratio between the quantum yields of the direct and backward process determines the product yield Q at the photostationary state[52], as shown in Eq. 5.

$$Q = \frac{[c]_\infty}{[c]_\infty + [t]_\infty} = \frac{J_{t\to c}}{J_{c\to t} + J_{t\to c}} = \frac{\varepsilon_t \Phi_{t\to c}}{\varepsilon_c \Phi_{c\to t} + \varepsilon_t \Phi_{t\to c}} \tag{5}$$

where t and c refer to the *trans* and *cis* isomers respectively, J is the reaction rate, ε is the molar extinction coefficient integrated over the excitation wavelength window and Φ is the quantum yield. The quantities $[c]_\infty$, $[t]_\infty$ are the asymptotic concentrations of the *cis* and *trans* isomers respectively, that in this framework correspond to the *cis* and *trans* populations at the end of the dynamics. The ratio between the molar extinction coefficients depends on the excitation wavelength and we shall assume $\varepsilon_t/\varepsilon_c = 7.9$ as determined by their integral average over the present excitation interval from the experimental data of azobenzene in methanol[52]. Such ratio impacts the position of the photostationary state, allowing to shift it selectively towards the *cis* and *trans* isomer depending on the irradiation wavelength. Nevertheless, the tunability is limited by the quantum yields of the individual processes, according to eq. 5. Aiming to manipulate the photostationary state position in azobenzene photoisomerization, we focus on improving the quantum yield of the unfavoured process, namely the *trans*→*cis* photoisomerization.

To perform the polaritonic photoisomerization simulations, we exploit an on-the-fly surface hopping approach[44, 53, 54, 55] and take into account all the nuclear degrees of freedom of azobenzene. Within this framework, the nuclear wavepacket moving on the polaritonic PESs is mimicked by a swarm of independent classical nuclear trajectories (see Methods).

To build the polaritonic states, we sought a field frequency to maximize the quantum yields for the $\pi - \pi^*$ *trans*→*cis* photoisomerization. We set the cavity resonant frequency to 2.80 eV, which allows to modify the crucial region of the first excited state at nearly planar transoid geometries (detailed in Figure 2c), *i.e.* the region of the PESs where the geometry of the molecule starts to partially twist but it is essentially trans. The coupling strength E_{1ph} is 0.002 au, corresponding to a splitting of ∼100 meV with a transition dipole of ∼1 a.u for the present case, consistent the observed 80-100 meV in the experiment by Baumberg and coworkers.[17] We sample the ground state distribution at thermostated[34] room temperature. For each sampled configuration, we mimic the excitation by near-UV light, with central wavelength of 313 nm (3.96 eV) and a full bandwidth of 1 eV. The excitation window is chosen to include the absorption spectral features corresponding to the first $\pi \rightarrow \pi^*$ transitions of trans- and cis-azobenzene, though a narrower excitation bandwidth centered at the same frequency yields the same results (see Supplementary Note 1 and Figure 3). Upon the absorption, the trajectories are vertically excited from the ground state to the polaritonic states. The excitation procedure is described in the Methods section[56]. The polaritonic states initially populated are $|R_3\rangle$, $|R_4\rangle$ and $|R_5\rangle$ which correspond essentially to $|S_2, 0\rangle$, $|S_3, 0\rangle$ and $|S_4, 0\rangle$ in the Franck Condon region. Their populations at time t=0 are 0.76 and 0.21 and 0.03 respectively. In the zero coupling case, the initial populations of the corresponding S_2, S_3 are 0.78 and 0.22, while S_4 is empty.

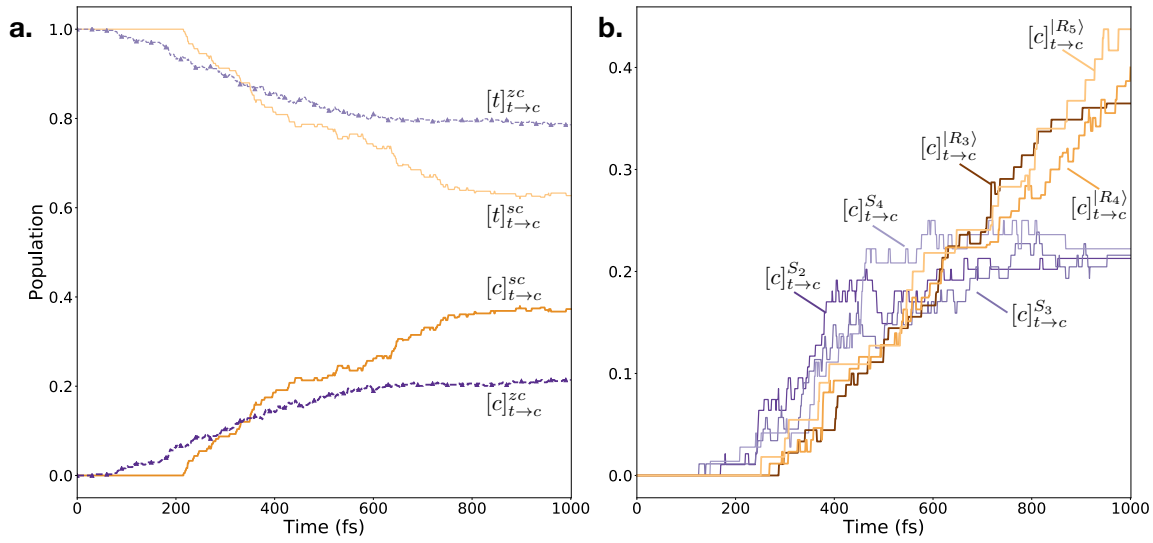

Figure 3: **Product-enriched *trans*→*cis* photoisomerization of azobenzene under strong coupling a)** Populations of azobenzene *trans* (light) and *cis* (dark) isomers in the zero coupling (purple) and strong coupling (orange) cases for the *trans*→*cis* $\pi - \pi^*$ photoisomerization, computed with a photon energy E_{ph} of 2.8 eV and a coupling strength E_{1ph} equal to 0.002 au. **b)** Comparison between the *cis* formation for processes starting on different electronic/polaritonic states in zero coupling (purple) and strong coupling (orange).The individual processes are investigated by running ∼100 trajectories. For each couple of initial states in zero coupling and strong coupling, the same sampling is used, *i.e.* $|R_3\rangle$ with $|S_2\rangle$, $|R_4\rangle$ with S_3, $|R_5\rangle$ with S_4.

The polaritonic non-adiabatic dynamics simulations results are reported in Figure 3 (see Supplementary Movies 1 and 2 for the dynamics with strong and zero coupling along the reactive coordinates). The capability of strong coupling to affect photochemistry is strikingly evident in Figure 3a, where we compare the population of *trans* and *cis* isomers for the *trans*→*cis* photoisomerization process obtained by the zero and strong coupling. Such populations are evaluated at each time step by counting the number of trajectories with a CNNC dihedral greater (*trans*) and smaller (*cis*) than 90°. The populations are then normalized to the total number of trajectories.

Remarkably, the *cis* formation is significantly more efficient for the strong coupling. This

is one of the main results of the present work, as the enhancement of a realistic reaction via electronic strong coupling has not been reported so far. As a first step to analyze the mechanism driving such increased yield of product, in Figure 3b we plot the fraction of reactive trajectories (reaching $CNNC < 90°$) for each starting state separately. Each of such individual processes in strong coupling (orange lines) is indeed more efficient than the corresponding one in zero coupling (purple lines). The strong coupling processes are on the average slower compared to the zero coupling case, *i.e.* the torsion around the N=N double bond is delayed, together with the decay to the ground state (Figure4a and 4b). Although paradoxically contrasting with the higher yields observed with respect to the zero coupling case, the slower dynamics offers a first hint to explain the change in the mechanism brought about by the strong coupling regime, as detailed later in this work. (See Supplementary Movie 3 for an example of the dynamics along a reactive trajectory).

The factor capable of both slowing the kinetics and increasing the quantum yields in polaritonic processes is the existence of the $|S_0, 1\rangle$ state and its coupling with $|S_0, 1\rangle$. Aiming to characterize the nature of the polaritonic states involved in the dynamics and to obtain a more meaningful comparison with the zero-coupling case, it is convenient to investigate the processes on the uncoupled state basis. To this aim, Figure 4a compares the uncoupled states populations (full lines) with those of the corresponding states in the zero coupling simulation (dashed lines, circle markers). Here, the population of the $|S_2, 0\rangle$, $|S_3, 0\rangle$ and $|S_4, 0\rangle$ manifold is represented as P_{sum} to highlight the relevant processes. The first striking difference is that the S_1 state in the zero coupling case is populated quicker than in the strong coupling case. In addition, a longer permanence of the trajectories on the $|S_1, 0\rangle$ states is observed in strong coupling, mainly because part of the population oscillates between $|S_1, 0\rangle$ to $|S_0, 1\rangle$ (see Table S1). Consequently, $|S_1, 0\rangle$ (strong coupling) can be found still populated at times where S_1 (zero coupling) is al-

ready decayed (see Figure 4a). The role of the $|S_0, 1\rangle$ state in delaying the depletion of $|S_1, 0\rangle$ is to act as a supplementary reservoir for the $|S_1, 0\rangle$ population during the first 400 fs. In fact, non-radiative electronic state decays from $|S_0, 1\rangle$ are blocked since the molecule is in its ground state.

The shape of the $|R_1\rangle$ and $|R_2\rangle$ PESs (see Figure 2) in the transoid region explains why the torsion is initially delayed in the strong coupling case. Most of the hops that populate these two states go from $|R_3\rangle$ to $|R_2\rangle$ (i.e. essentially $|S_2, 0\rangle \rightarrow |S_1, 0\rangle$). Subsequently, more hops back and forth between $|R_1\rangle$ and $|R_2\rangle$ occur, due to the avoided crossing involving $|S_1, 0\rangle$ and $|S_0, 1\rangle$ (see Table S1). The upper surface, belonging to $|R_2\rangle$, is less favourable than that of $|R_1\rangle$ to the torsional and the symNNC motions (see Figure 2b), *i.e.* to the decrease of the CNNC dihedral and to the increase of both NNC angles. By partially populating $|R_2\rangle$, the progress along the reaction coordinate CNNC and the symNNC vibrational excitation are both hindered.

The association of slower torsonal motion and slower $|S_1, 0\rangle$ decay with higher $\Phi_{t\rightarrow c}$ quantum yield, which characterizes the strong coupling with respect to the zero coupling case, is not so intuitive. Still, this effect is reminiscent of the same joint trends observed in simulations of the *trans*→*cis* photoisomerization in solvents of increasing viscosity, in agreement with experimental quantum yields and fluorescence lifetimes for the field-free case[48]. A similar hindrance of the motion along the reaction coordinate, caused by strong coupling, was highlighted by Galego et al[57] by full quantum simulations, but unavoidably led to suppression of the photoisomerization due to the one-dimensional model.

The reason why a slower progress along the reaction coordinate leads to a higher quantum yield for the realistic model we are using here can be found in the shape of the S_1, S_0 cross-

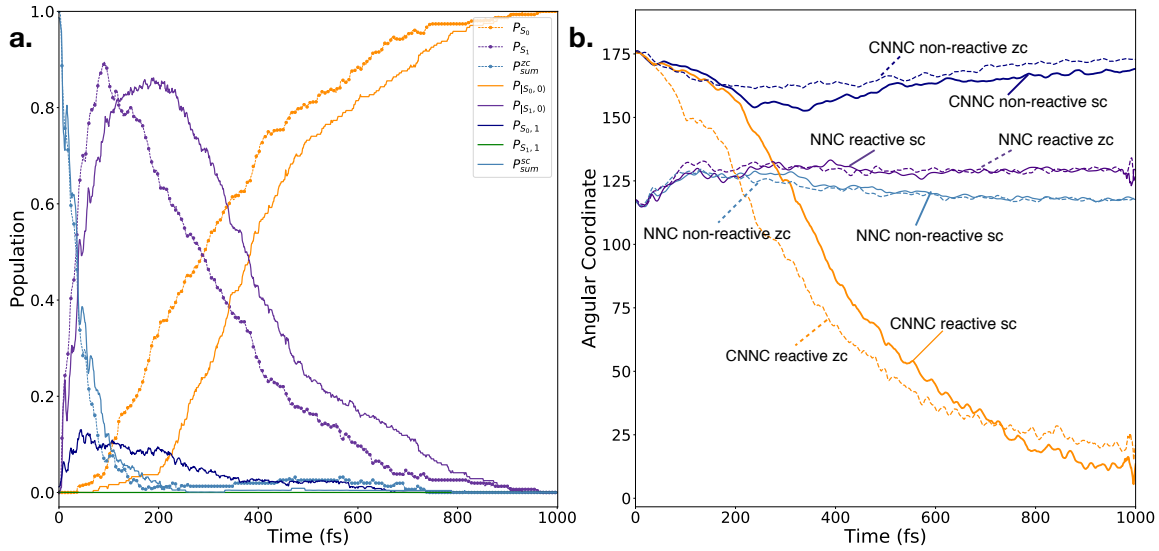

Figure 4: **Population and geometrical relaxation dynamics upon photoisomerizationa)** Population evolution on the uncoupled states in strong coupling (full lines), directly compared to the zero coupling population evolution involving the same states (dashed lines with markers). The strong coupling population evolution is slowed by the presence of $|S_0, 1\rangle$ (blue full line), which is transiently populated during the dynamics. **b)** CNNC and NNC angles averaged over the reactive and non-reactive trajectories in zero coupling (dashed lines) and strong coupling (full lines), computed as a function of time.The upper surface, belonging to $|R_2\rangle$, is less favourable than that of $|R_1\rangle$ to the torsional and the symNNC motions, *i.e.* to the decrease of the CNNC dihedral and to the increase of both NNC angles. Therefore, by partially populating $|R2\rangle$ the progress along the reaction coordinate CNNC and the symNNC vibrational excitation are both hindered. See Supplementary Note 4 for the corresponding cis-trans plot.

ing seam. Note that, after leaving the surroundings of the Franck-Condon region by twisting the N=N bond and/or increasing the symNNC angles, $|R_1\rangle$ becomes almost pure $|S_1, 0\rangle$. In the new region, its energy gets closer to that of $|R_0\rangle$: a crossing seam between the two PESs exists. Even more, the crossing seam is practically unaltered with respect to the zero-coupling case (see Supplementary Note 4 of the present work and Figure 1 in ref. [48]). Although the energy minimum of such seam (optimized conical intersection, CoIn) is found at a twisted geometry (CNNC=95°), the seam is also accessible at larger CNNC values by opening the symNNC bond angles. In zero coupling, the symNNC bending mode is excited once the S_1 state is populated by

internal conversion from S_2, explainable by comparing the equilibrium values of the NNC angles in S_1 and in S_0/S_2 (132° versus 118° and 110° at planar geometries). This excitation results in the periodic opening of the symNNC angle and, in turn, promotes the internal conversion of S_1 to the ground state by making the seam accessible at transoid regions, resulting in a rather low *trans*→*cis* photoisomerization quantum yield. On the contrary in strong coupling, the hindering of the twisting and bending motions discussed above decreases the extent of symNNC excitation. In fact, with more time spent at transoid geometries, symNNC is also quenched by vibrational energy transfer to other internal modes and to the medium. As such, the detrimental effect of the symNNC on the trans-cis photoisomerization quantum yield is partially suppressed.

The behaviour hereby described is well highlighted in Figure 5, where we compare the distribution of the geometrical coordinates at the moment of the S_1-S_0 ($|R_1\rangle - |R_0\rangle$) hopping in zero coupling (strong coupling), depicted for the non-reactive and reactive trajectories in the upper and lower panels respectively. Quantitative data, including the hopping times, are also provided in Table S1.

The reactive trajectories are shown to hop at CNNC closer to 90°, while the non-reactive ones count many hops at large values of both CNNC and symNNC. Moreover, a significantly wider distribution of symNNC is observed for the zero coupling case (purple), signature that the symNNC is more excited in zero coupling than in strong coupling. Large symNNC (symNNC$>150°$) in zero coupling are accompanied by many hops at CNNC$>130°$, confirming that the excitation of symmetric NNC vibration promotes the internal conversion at transoid geometries. The narrower interval of symNNC for the strong coupling case, instead, allows the trajectories to hop at averagely more twisted geometries, accompanied by a higher probability of successful photoconversion to the cis isomer.

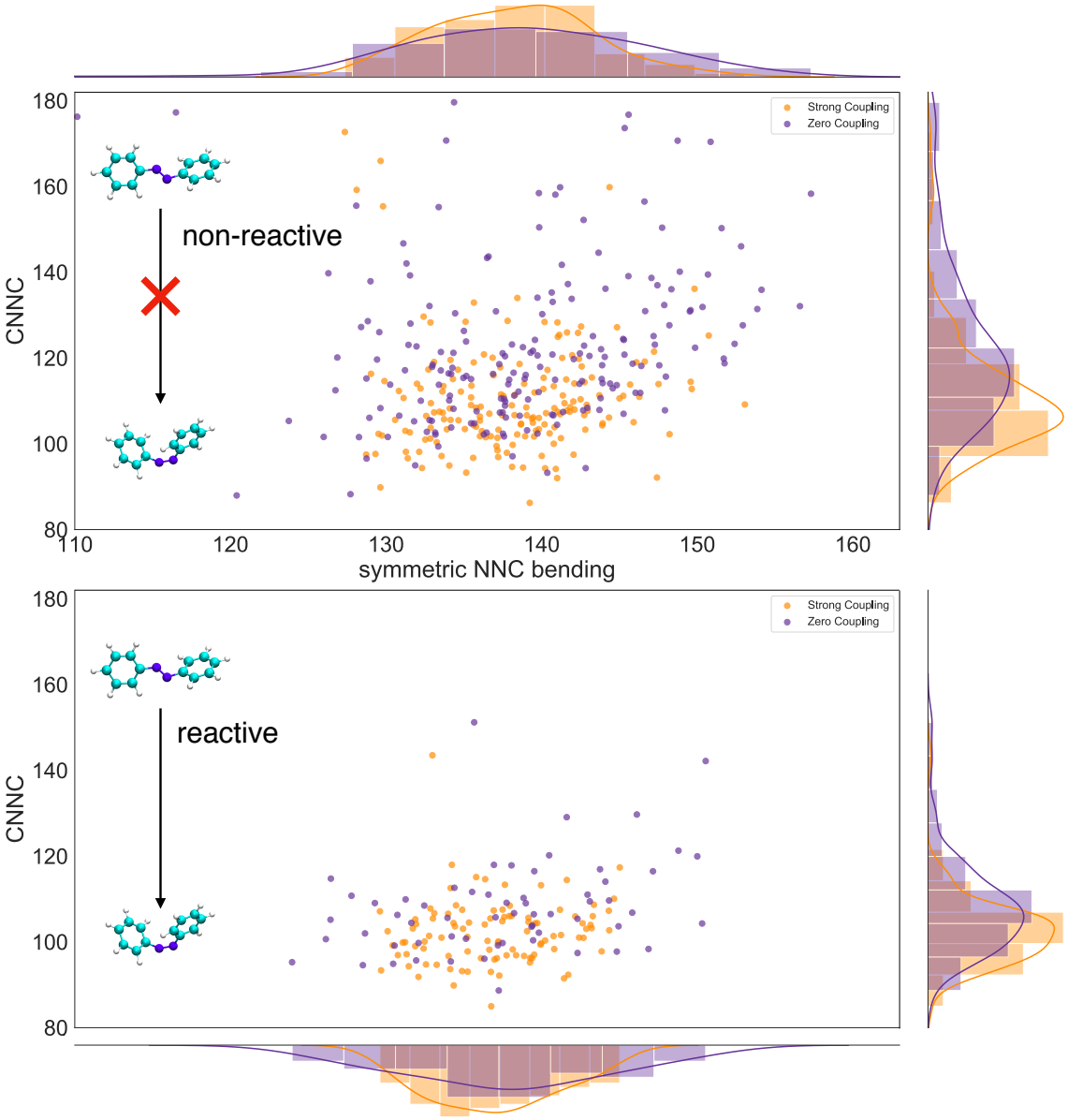

Figure 5: **Non-reactive/Reactive photoisomerization dynamics for strong coupling and zero-field upon $S_1 - S_0$ hopping**Non-reactive (upper) and reactive (lower) distributions of the reactive coordinates (symNNC, CNNC), computed upon the $S_1 - S_0$ hops for the zero-field case (purple) and $|R_1\rangle - |R_0\rangle$ for the strong coupling case (orange). The distributions, in particular the non-reactive one, show that high excitation of symNNC causes hops at less twisted CNNC values, resulting in a lower photoisomerization yield in zero coupling with respect to strong coupling.

Until now, we have shown that the coherent exchange of energy between light and matter impacts both the kinetics of the dynamics and the mechanism, resulting in a non-trivial trend in the quantum yields. To verify the consequence of this result on photostationary *cis*/*trans* populations, the *cis*→*trans* photoreaction at the same excitation frequency must be simulated as well. We found that such process in strong coupling shows the same yield with respect to the zero coupling case, $\Phi_{c\to t} = 58\%$ and $\Phi_{c\to t} = 61\%$ respectively. This is consequent to the more favourable slope of the PESs in the *cis* side, which also makes the *cis*→*trans* photoisomerization quantum yield insensitive to environmental hindrances[48, 49, 51]. Going from the cis to the trans isomer, such steep PESs make the effect of the $|S_0, 1\rangle$ state in the dynamics almost irrelevant, resulting in the *cis*→*trans* photoisomerization occurring on much shorter timescales (150 fs, see Supplementary Note 4) than in the *trans*→*cis*. Therefore, the substantial rise of the yields in the *trans*→*cis* process is sufficient to push the photostationary state towards the *cis* isomer.

When the system is in its free-photon state $|n, 1\rangle$, a loss of the photon can occur (*e.g.* by leakage from the cavity or absorbed by the cavity walls). As a consequence, the coherent exchange between light and matter is disrupted and the molecule collapses from a mixture of $|n', 0\rangle$ and $|n, 1\rangle$ state to $|n, 0\rangle$ only (see Methods).

To test how robust the results seen above are with respect to photonic losses in the resonant cavity, we simulated the *trans*→*cis* and *cis*→*trans* photoisomerization processes in presence of a finite cavity lifetime τ_{cav} and compared the so-obtained quantum yields to the zero coupling case (see Figure 6). The photostationary state yield of cis product exceeds the zero coupling one for $\tau_{cav} \geq 50$ fs (Figure 6a). Remarkably, this time is much shorter than the typical photoisomerization timescale, while intuitively one would expect that cavity lifetimes comparable to

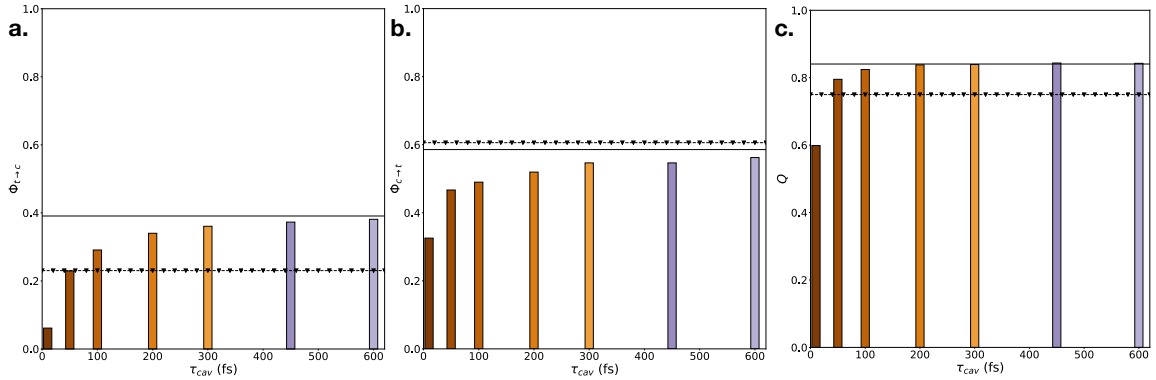

Figure 6: **Effect of cavity losses on the photostationary state** Quantum yields comparison for the **a)** *trans*→*cis* and **b)** *cis*→*trans* isomerization in strong coupling as a function of the cavity photon lifetime. The black dotted line is the zero coupling limit, while the full line is the lossless cavity limit. The transient role of $|S_0, 1\rangle$ is reflected by lower quantum yields for very lossy cavities with respect to the zero coupling case. **c)** The product yield at the photostationary state computed by taking into account the forward and backward reaction. The molar extinction coefficients are obtained by their integral average over the present excitation interval, starting from the experimental data reported by Vetrakova and collaborators[52]. The product yield Q at the photostationary state is shifted towards the strong coupling limit for τ_{cav} greater than 50 fs.

the photoisomerization time are needed to observe enhanced reactions. The photosiomerization timescales are longer than the permanence time of the trajectories on the $|S_0, 1\rangle$, which is the only $|n, 1\rangle$ state with a non-negligible population at any time. While the decay to the ground state and the photoisomerization take around 800 fs to be completed, the average permanence time in $|S_0, 1\rangle$ can be estimated to about 35 fs from its time-dependent population. We see then why a photonic loss timescale much shorter than the timescale of the whole photochemical process is compatible with the observation of strong coupling effects. Below 100 fs, however, the *trans*→*cis* conversion yield is quite sensitive to τ_{cav}. Instead, the *cis*→*trans* one is less affected due to the more favourable slope of te PESs and the faster photoisomerization dynamics (see Figures 2 and Supplementary Note 4).

Discussion/Conclusions

By building the polaritonic states of azobenzene, we have shown how the molecular complexity can be taken into account for a single molecule strongly coupled to a resonator. The inclusion of a detailed treatment for the molecule and its environment allowed us to investigate the shape of single-molecule polaritons when a manifold of excited states is involved in the strong coupling.

We have shown that strong coupling deeply affects the dynamical processes taking place on polaritonic PESs. In particular, we have found a remarkable increase of the quantum yield for the $\pi - \pi^*$ *trans*→*cis* photoisomerization, due to subtle changes in the mechanism: the shape of the polaritonic PESs and the time spent in the one-photon states bring about a lower degree of excitation of the symmetric NNC bending vibration, that is the main cause of early decay from the S_1 state in zero-coupling conditions. As a result, under strong coupling more molecules reach a torsion of the N=N bond closer to cis before relaxing to the ground state and thus photoisomerize with a higher probability. By taking into account the backward reaction (*cis*→*trans*), such effect results in an increase of the photostationary concentration of the *cis* isomer.

Through the simulation of a realistic system, *i.e.* by including the effects of environment and cavity losses, we could estimate a minimum cavity lifetime of 50 fs to observe a shift of the photostationary equilibrium towards higher *trans*→*cis* photoconversions. Although currently the lifetimes of the typical plasmonic nanocavities struggle to exceed the 10 fs, new experiments are actively devising prototypical setups to achieve high reproducibility[17, 19, 20] and longer lifetimes for these systems[21, 58] at the single molecule level. The quickly growing interest in polaritonic applications bodes well for polaritonic devices to be exploited in real-life polaritonic chemistry.

Our results show promising possibilities in this field. Among them, the enhancement of the quantum yields and photostationary concentrations in experimentally achievable systems opens up a pathway towards a real control of photochemical reactions (*i.e.* quenching and enhancement). Concerning the role of polaritons in the photochemistry of single molecules, we think that the physics of polariton-mediated reactivity is far from being thoroughly investigated. Among the yet-to-explore possibilities we mention multistate and bielectronic polaritonic processes, such as photoreactions mediated by excitation transfer.

Methods

Strong coupling Hamiltonian The Hamiltonian describing the system is given in eq. 1. Aiming to include all the degrees of freedom of azobenzene, we exploit a semiempirical AM1 Hamiltonian reparametrized for the first few electronic excited states of azobenzene[47]. In addition, it includes the molecular interaction with the environment (see next section). The basis on which we build the polaritonic states is the set of electronic-adiabatic singlets $\{n\}$, from S_0 to S_4. The cavity Hamiltonian of the quantized electromagnetic field is:

$$\hat{H}_{cav} = \hbar\omega_{cav}\left(\hat{b}^\dagger\hat{b} + \frac{1}{2}\right) \tag{6}$$

where ω_{cav} is the resonator frequency and $\hat{b}^\dagger$, $\hat{b}$ are the bosonic creation and annihilation operators. As reported in the main text, the eigenvectors of the non-interacting Hamiltonian $\hat{H}_{mol}+\hat{H}_{cav}$ constitute the uncoupled state basis $\{|n,p\rangle\}$. To obtain the polaritonic states (eq. 4) and energies we select a subset of states $|n,p\rangle$ of interest, in which we perfom a CI calculation including the dipolar light-molecule interaction at QM level (eq. 2), working in the Coulomb gauge and long wavelength approximation. The stability of the dipolar approximation has been proven to break up when reaching high couplings [59, 60, 61, 62]. To prove the robustness of

such approximation in the current case, test calculations have been performed as in the previous work[44] (see Supplementary Note 3).

Inclusion of the environment The environment is included at QM/MM level interfaced with the electronic semiempirical Hamiltonian. The molecular Hamiltonian for the system is partitioned as[63]:

$$\hat{H}_{mol} = \hat{H}_{QM} + \hat{H}_{QM/MM} + \hat{H}_{MM}. \tag{7}$$

The QM part is composed by the azobenzene molecule, the MM part is composed by the cucurbit-7-uril molecule (150 atoms), 710 water molecules and eight frozen layers of gold encapsulating the system (418 atoms each, only van der Waals interactions). The force field used to evaluate the MM part is OPLS-AA contained in the TINKER code[64]. The QM/MM interactions are modelled by electrostatic embedding plus Lennard-Jones atom-atom potentials[51, 65, 66] (See Supplementary Note 1).

Surface Hopping on polaritonic states After building the molecule embedded in environment and optimizing the geometry at MM level, the starting wavepacket is sampled on the molecular ground state by a QM/MM dynamics. At the end of such dynamics, few hundreds of initial conditions (nuclear phase space point and polaritonic/electronic state) are extracted by evaluating the transition probability from the ground state to the S_2,S_3,S_4 electronic states (zero coupling) or $|R_3\rangle, |R_4\rangle, |R_5\rangle$ polaritonic states (strong coupling). Both the zero coupling and strong coupling states are excited within the same energy window, *i.e.* centered at 3.96 eV (from 3.46 eV to 4.46 eV). More details can be found in Supplementary Note 1.

The non-adiabatic molecular dynamics is perfomed by exploiting the Direct Trajectory Surface Hopping approach[53]. Few hundreds of classical nuclear trajectories (230 to 270) are

computed on-the-fly on the polaritonic PESs independently. The hopping probability between the states is a modified version of Tully's Fewest Switches[67]. The modifications added take into account the strong coupling contributions[44] and the decoherence corrections needed to properly describe the decoupling of wavepackets travelling on different states[54].

As usual in surface hopping, the population of a polaritonic state $|R_m\rangle$ is represented by the fraction of trajectories evolving on $|R_m\rangle$ (called the "current" state) at the given time. Consistently, the population of unmixed states $|n,p\rangle$, shown in Figure 4a, are obtained by averaging $\left|D^m_{n,p}\right|^2$ over the full swarm of trajectories, where $|R_m\rangle$ is again the current state.

Cavity Losses The decay probability to account for cavity losses is evaluated through a stochastic approach. In particular, it is taken to be proportional to the square of the coefficients of the uncoupled states $|n,p\rangle$, with $p > 0$ ($p = 1$ in the present work), composing the time-dependent polaritonic wavefunction (see equation 4):

$$P_{loss} = \sum_{n,p\geq 1}^{n_{st}} \frac{1}{\tau_{cav}} \Delta t \left| \sum_m C_m D^m_{n,p} \right|^2 = \sum_{n,p\geq 1}^{n_{st}} P_{|n,p\rangle}. \tag{8}$$

Here, τ_{cav} denotes the cavity lifetime while Δt is the integration timestep.

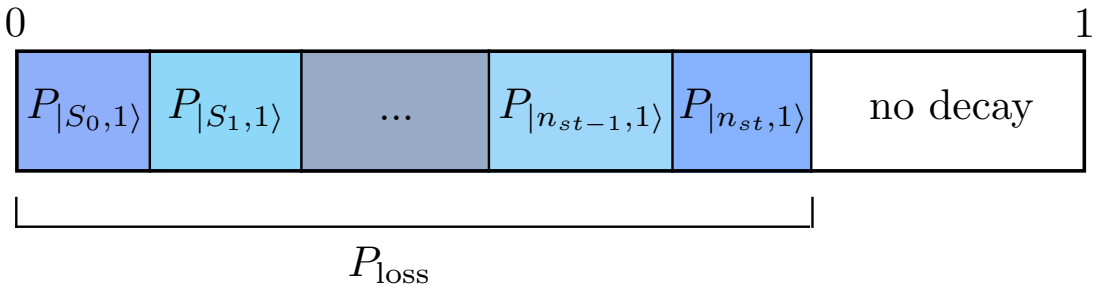

Figure 7: **Algorithm to include the photon loss probability—**

The decay probabilities referred to each state are indicated as $P_{|n,1\rangle}$ and n_{st} denotes the total number of electronic states included in the calculation. A uniform random number is generated

between 0 and 1 and compared to the above interval. A check if the random number falls in any sub interval up to $P|n_{st},1\rangle$ is performed. If that is the case, the photon is lost from $|n',1\rangle$. The decay operator $\hat{D}_{n'}$ is then applied to the polaritonic wavefunction:

$$\hat{D}_{n'}|\Psi\rangle = |n',0\rangle\langle n',1|\Psi\rangle. \tag{9}$$

The arrival state $|F\rangle$ is determined by taking the adiabatic state which has the largest overlap $\langle n',0|F\rangle$ with the electronic state $|n',0\rangle$. The dynamics is then resumed by taking $|F\rangle$ as the new current state. We hereby point out that, for our current work, the decay always occurs from the $|S_0,1\rangle$ state, as it is the only state with $p>0$ with a non-negligible population during the dynamics. Even more, the arrival state is always $|R_0\rangle$, as it is almost purely $|S_0,0\rangle$ at all the relevant geometries (see Supplementary Note 2). More generally, the wavefunction after the jump should be written as an electronic wavepacket, mantaining the possible electronic coherence present within the $p>0$ manifold.

Code Availability

The calculations were based on a locally modified version of MOPAC2002 and TINKER, and are available from G.G. and M.P. upon reasonable request. The analysis and the supplementary movies are based on *ad-hoc* tools which are available from J.F. upon request.

Acknowledgements

J.F. and S.C. acknowledge funding from the ERC under the grant ERC-CoG-681285 TAME-Plasmons. G.G. and M.P. acknowledge funding from the University of Pisa, PRA 2017 28 and PRA 2018 36.

Author Contributions

S.C. initiated this project; J.F., G.G., M.P. and S.C. designed the investigation; J.F. performed the calculations; all the authors contributed to the analysis of results and to the writing of the paper.

Declaration of interests

The authors declare no competing interests.

References

[1] Y. Fang and M. Sun, "Nanoplasmonic waveguides: towards applications in integrated nanophotonic circuits," *Light: Science &Amp; Applications*, vol. 4, p. 294, 2015.

[2] A. B. Dahlin, N. J. Wittenberg, F. Höök, and S.-H. Oh, "Promises and challenges of nanoplasmonic devices for refractometric biosensing," *Nanophotonics*, vol. 2, pp. 83–101, 2013.

[3] M. I. Stockman, "Ultrafast nanoplasmonics under coherent control," *New Journal of Physics*, vol. 10, p. 025031, 2008.

[4] K. J. Savage, M. M. Hawkeye, R. Esteban, A. G. Borisov, J. Aizpurua, and J. J.Baumberg, "Revealing the quantum regime in tunnelling plasmonics," *Nature*, vol. 491, p. 574, 11 2012.

[5] M. I. Stockman, M. F. Kling, U. Kleineberg, and F. Krausz, "Attosecond nanoplasmonic-field microscope," *Nature Photonics*, vol. 1, p. 539, 2007.

[6] D. Punj, M. Mivelle, S. B. Moparthi, T. S. van Zanten, H. Rigneault, N. F. van Hulst, M. F. García-Parajó, and J. Wenger, "A plasmonic 'antenna-in-box' platform for enhanced

single-molecule analysis at micromolar concentrations," *Nature Nanotechnology*, vol. 8, p. 512, 2013.

[7] C. Barner-Kowollik, M. Bastmeyer, E. Blasco, G. Delaittre, P. Müller, B. Richter, and M. Wegener, "3d laser micro- and nanoprinting: Challenges for chemistry," *Angewandte Chemie International Edition*, vol. 56, no. 50, pp. 15828–15845, 2017.

[8] T. H. Taminiau, F. D. Stefani, F. B. Segerink, and N. F. van Hulst, "Optical antennas direct single-molecule emission," *Nature Photonics*, vol. 2, p. 234, 2008.

[9] T. H. Taminiau, F. D. Stefani, and N. F. van Hulst, "Optical nanorod antennas modeled as cavities for dipolar emitters: Evolution of sub- and super-radiant modes," *Nano Letters*, vol. 11, no. 3, pp. 1020–1024, 2011.

[10] J. T. Hugall, A. Singh, and N. F. van Hulst, "Plasmonic cavity coupling," *ACS Photonics*, vol. 5, no. 1, pp. 43–53, 2018.

[11] E. T. Jaynes and F. W. Cummings, "Comparison of quantum and semiclassical radiation theories with application to the beam maser," *Proc. IEEE*, vol. 51, p. 89, 1963.

[12] J. Flick, M. Ruggenthaler, H. Appel, and A. Rubio, "Atoms and molecules in cavities, from weak to strong coupling in quantum-electrodynamics (qed) chemistry," *Proc. Natl. Acad. Sci. USA*, vol. 114, no. 12, p. 3026, 2017.

[13] J. Galego, F. J. Garcia-Vidal, and J. Feist, "Cavity-induced modifications of molecular structure in the strong-coupling regime," *Phys. Rev. X*, vol. 5, p. 041022, 2015.

[14] T. Neuman, R. Esteban, D. Casanova, F. J. García-Vidal, and J. Aizpurua, "Coupling of molecular emitters and plasmonic cavities beyond the point-dipole approximation," *Nano Letters*, vol. 18, pp. 2358–2364, 2018.

[15] T. Schwartz, J. A. Hutchison, C. Genet, and T. W. Ebbesen, "Reversible switching of ultrastrong light-molecule coupling," *Phys. Rev. Lett.*, vol. 106, pp. 196405–196409, 2011.

[16] J. A. Hutchison, T. Schwartz, C. Genet, E. Devaux, and T. W. Ebbesen,"Modifying chemical landscapes by coupling to vacuum fields," *Angew. Chem. Int. Ed.*, vol. 51, p. 1592, 2012.

[17] R. Chikkaraddy, B. de Nijs, F. Benz, S. J. Barrow, O. A. Scherman, E. Rosta, A. Demetriadou, P. Fox, O. Hess, and J. J. Baumberg, "Single-molecule strong coupling at room temperature in plasmonic nanocavities," *Nature*, vol. 535, p. 127, 2016.

[18] N. Kongsuwan, A. Demetriadou, R. Chikkaraddy, F. Benz, V. A. Turek, U. F. Keyser, J. J. Baumberg, and O. Hess, "Suppressed quenching and strong-coupling of purcell-enhanced single-molecule emission in plasmonic nanocavities," *ACS Photonics*, vol. 5, pp. 186–191, 2018.

[19] R. Chikkaraddy, V. A. Turek, N. Kongsuwan, F. Benz, C. Carnegie, T. van de Goor, B. de Nijs, A. Demetriadou, O. Hess, U. F. Keyser, and J. J. Baumberg, "Mapping nanoscale hotspots with single-molecule emitters assembled into plasmonic nanocavities using dna origami," *Nano Letters*, vol. 18, pp. 405–411, 2018.

[20] O. S. Ojambati, R. Chikkaraddy, W. D. Deacon, M. Horton, D. Kos, V. A. Turek, U. F. Keyser, and J. J. Baumberg, "Quantum electrodynamics at room temperature coupling a single vibrating molecule with a plasmonic nanocavity," *Nature Communications*, vol. 10, no. 1, p. 1049, 2019.

[21] D. Wang, H. Kelkar, D. Martin-Cano, T. Utikal, S. Götzinger, and V. Sandoghdar, "Coherent coupling of a single molecule to a scanning fabry-perot microcavity," *Phys. Rev. X*, vol. 7, pp. 021014–021022, 2017.

[22] J. Flick, N. Rivera, and P. Narang, "Strong light-matter coupling in quantum chemistry and quantum photonics," *Nanophotonics*, vol. 7, no. 1, 2018.

[23] R. F. Ribeiro, L. A. Martínez-Martínez, M. Du, J. Campos-Gonzalez-Angulo, and J. Yuen-Zhou, "Polariton chemistry: controlling molecular dynamics with optical cavities," *Chem. Sci.*, vol. 9, pp. 6325–6339, 2018.

[24] J. A. Hutchison, A. Liscio, T. Schwartz, A. Canaguier-Durand, C. Genet, V. Palermo, P. Samor, and T. W. Ebbesen, "Tuning the work-function via strong coupling," *Advanced Materials*, vol. 25, no. 17, pp. 2481–2485, 2013.

[25] A. Fontcuberta i Morral and F. Stellacci, "Ultrastrong routes to new chemistry," *Nature Materials*, vol. 11, p. 272, 2012.

[26] Y. Zhang, Q.-S. Meng, L. Zhang, Y. Luo, Y.-J. Yu, B. Yang, Y. Zhang, R. Esteban, J. Aizpurua, Y. Luo, J.-L. Yang, Z.-C. Dong, and J. G. Hou, "Sub-nanometre control of the coherent interaction between a single molecule and a plasmonic nanocavity," *Nat. Comm.*, vol. 8, p. 15225, 2017.

[27] K. Bennett, M. Kowalewski, and S. Mukamel, "Novel photochemistry of molecular polaritons in optical cavities," *Faraday Discuss.*, vol. 194, p. 259, 2016.

[28] J. Feist, J. Galego, and F. J. Garcia-Vidal, "Polaritonic chemistry with organic molecules," *ACS Photonics*, vol. 5, p. 205, 2018.

[29] S. Strauf, "Lasing under strong coupling," *Nature Physics*, vol. 6, p. 244, 2010.

[30] R. Sawant and S. A. Rangwala, "Lasing by driven atoms-cavity system in collective strong coupling regime," *Scientific Reports*, vol. 7, p. 11432, 2017.

[31] W. Du, S. Zhang, J. Shi, J. Chen, Z. Wu, Y. Mi, Z. Liu, Y. Li, X. Sui, R. Wang, X. Qiu, T. Wu, Y. Xiao, Q. Zhang, and X. Liu, "Strong exciton–photon coupling and lasing behavior in all-inorganic cspbbr3 micro/nanowire fabry-pérot cavity," *ACS Photonics*, vol. 5, pp. 2051–2059, 2018.

[32] C. Gies, M. Florian, P. Gartner, and F. Jahnke, "The single quantum dot-laser: lasing and strong coupling in the high-excitation regime," *Opt. Express*, vol. 19, pp. 14370–14388, 2011.

[33] L. Garziano, A. Ridolfo, S. De Liberato, and S. Savasta, "Cavity qed in the ultrastrong coupling regime: Photon bunching from the emission of individual dressed qubits," *ACS Photonics*, vol. 4, pp. 2345–2351, 2017.

[34] G. Bussi, D. Donadio, and M. Parrinello, "Canonical sampling through velocity rescaling," *J. Chem. Phys*, vol. 126, no. 1, p. 014101, 2007.

[35] O. Vendrell, "Coherent dynamics in cavity femtochemistry: Application of the multi-configuration time-dependent hartree method," *Chemical Physics*, vol. 509, pp. 55 – 65, 2018.

[36] H. L. Luk, J. Feist, J. J. Toppari, and G. Groenhof, "Multiscale molecular dynamics simulations of polaritonic chemistry," *Journal of Chemical Theory and Computation*, vol. 13, no. 9, pp. 4324–4335, 2017.

[37] G. J. Halász, Á. Vibók, and L. S. Cederbaum, "Direct signature of light-induced conical intersections in diatomics," *The Journal of Physical Chemistry Letters*, vol. 6, pp. 348–354, 2015.

[38] T. Szidarovszky, G. J. Halász, A. G. Császár, L. S. Cederbaum, and Á. Vibók, "Conical intersections induced by quantum light: Field-dressed spectra from the weak to the ul-

trastrong coupling regimes," *The Journal of Physical Chemistry Letters*, vol. 9, no. 21, pp. 6215–6223, 2018.

[39] M. Kowalewski, K. Bennett, and S. Mukamel, "Non-adiabatic dynamics of molecules in optical cavities," *J. Chem. Phys.*, vol. 144, p. 054309, 2016.

[40] L. A. Martínez-Martínez, M. Du, R. F. Ribeiro, S. Kéna-Cohen, and J. Yuen-Zhou, "Polariton-assisted singlet fission in acene aggregates," *The Journal of Physical Chemistry Letters*, vol. 9, no. 8, pp. 1951–195u, 2018.

[41] R. Sáez-Blázquez, J. Feist, A. I. Fernández-Domínguez, and F. J. García-Vidal, "Organic polaritons enable local vibrations to drive long-range energy transfer," *Phys. Rev. B*, vol. 97, p. 241407, Jun 2018.

[42] M. Du, R. F. Ribeiro, and J. Yuen-Zhou, "Remote control of chemistry in optical cavities," *Chem*, vol. 5, pp. 1167–1181, 2019/08/19 2019.

[43] J. Galego, F. J. Garcia-Vidal, and J. Feist, "Many-molecule reaction triggered by a single photon in polaritonic chemistry," *Phys. Rev. Lett.*, vol. 119, p. 136001, Sep 2017.

[44] J. Fregoni, G. Granucci, E. Coccia, M. Persico, and S. Corni, "Manipulating azobenzene photoisomerization through strong light–molecule coupling," *Nature Communications*, vol. 9, no. 1, p. 4688, 2018.

[45] T. Cusati, G. Granucci, M. Persico, and G. Spighi, "Oscillator strength and polarization of the forbidden n* band of trans-azobenzene: A computational study," *The Journal of Chemical Physics*, vol. 128, no. 19, p. 194312, 2008.

[46] G. Granucci and A. Toniolo, "Molecular gradients for semiempirical ci wavefunctions with floating occupation molecular orbitals," *Chemical Physics Letters*, vol. 325, pp. 79–85, 2000.

[47] T. Cusati, G. Granucci, E. Martínez-Núñez, F. Martini, M. Persico, and S. Vázquez, "Semiempirical hamiltonian for simulation of azobenzene photochemistry," *J. Phys. Chem. A*, vol. 116, p. 98, 2012.

[48] T. Cusati, G. Granucci, and M. Persico, "Photodynamics and time-resolved fluorescence of azobenzene in solution: A mixed quantum-classical simulation," *Journal of the American Chemical Society*, vol. 133, no. 13, pp. 5109–5123, 2011.

[49] V. Cantatore, G. Granucci, and M. Persico, "Simulation of the photodynamics of azobenzene: Decoherence and solvent effects," *Computational and Theoretical Chemistry*, vol. 1040-1041, pp. 126–135, 2014.

[50] L. Favero, G. Granucci, and M. Persico, "Surface hopping investigation of benzophenone excited state dynamics," *Phys. Chem. Chem. Phys.*, vol. 18, pp. 10499–10506, 2016.

[51] E. Benassi, G. Granucci, M. Persico, and S. Corni, "Can azobenzene photoisomerize when chemisorbed on a gold surface? an analysis of steric effects based on nonadiabatic dynamics simulations," *The Journal of Physical Chemistry C*, vol. 119, pp. 5962–5974, 03 2015.

[52] Ľ. Vetráková, V. Ladányi, J. Al Anshori, P. Dvořák, J. Wirz, and D. Heger, "The absorption spectrum of cis-azobenzene," *Photochem. Photobiol. Sci.*, vol. 16, pp. 1749–1756, 2017.

[53] G. Granucci, M. Persico, and A. Toniolo, "Direct semiclassical simulation of photochemical processes with semiempirical wave functions," *J. Chem. Phys.*, vol. 114, no. 24, p. 10608, 2001.

[54] G. Granucci, M. Persico, and A. Zoccante, "Including quantum decoherence in surface hopping," *J. Chem. Phys.*, vol. 133, no. 13, p. 134111, 2010.

[55] J. J. Bajo, G. Granucci, and M. Persico, "Interplay of radiative and nonradiative transitions in surface hopping with radiation-molecule interactions," *J. Chem. Phys.*, vol. 140, no. 4, p. 044113, 2014.

[56] M. Persico and G. Granucci, "An overview of nonadiabatic dynamics simulations methods, with focus on the direct approach versus the fitting of potential energy surfaces," *Theoretical Chemistry Accounts*, vol. 133, p. 1526, Jul 2014.

[57] J. Galego, F. J. Garcia-Vidal, and J. Feist, "Suppressing photochemical reactions with quantized light fields," *Nature Communications*, vol. 7, p. 13841, 2016.

[58] D. Rattenbacher, A. Shkarin, J. Renger, T. Utikal, S. Götzinger, and V. Sandoghdar, "Coherent coupling of single molecules to on-chip ring resonators," *New Journal of Physics*, vol. 21, p. 062002, jun.

[59] D. De Bernardis, T. Jaako, and P. Rabl, "Cavity quantum electrodynamics in the nonperturbative regime," *Phys. Rev. A*, vol. 97, p. 043820, Apr 2018.

[60] D. De Bernardis, P. Pilar, T. Jaako, S. De Liberato, and P. Rabl, "Breakdown of gauge invariance in ultrastrong-coupling cavity qed," *Phys. Rev. A*, vol. 98, p. 053819, Nov 2018.

[61] A. Stokes and A. Nazir, "Gauge ambiguities imply jaynes-cummings physics remains valid in ultrastrong coupling qed," *Nature Communications*, vol. 10, no. 1, p. 499, 2019.

[62] O. Di Stefano, A. Settineri, V. Macrì, L. Garziano, R. Stassi, S. Savasta, and F. Nori, "Resolution of gauge ambiguities in ultrastrong-coupling cavity quantum electrodynamics," *Nature Physics*, 2019.

[63] A. Warshel and M. Levitt, "Theoretical studies of enzymic reactions: Dielectric, electrostatic and steric stabilization of the carbonium ion in the reaction of lysozyme," *Journal of Molecular Biology*, vol. 103, no. 2, pp. 227 – 249, 1976.

[64] J. W. Ponder and F. M. Richards, "An efficient newton-like method for molecular mechanics energy minimization of large molecules," *Journal of Computational Chemistry*, vol. 8, no. 7, pp. 1016–1024, 1987.

[65] A. Toniolo, C. Ciminelli, G. Granucci, T. Laino, and M. Persico, "Qm/mm connection atoms for the multistate treatment of organic and biological molecules," *Theoretical Chemistry Accounts*, vol. 111, no. 2, pp. 270–279, 2004.

[66] C. Ciminelli, G. Granucci, and M. Persico, "Are azobenzenophanes rotation-restricted?," *The Journal of Chemical Physics*, vol. 123, no. 17, p. 174317, 2005.

[67] J. C. Tully, "Molecular dynamics with electronic transitions," *The Journal of Chemical Physics*, vol. 93, no. 2, pp. 1061–1071, 1990.